2790 *Chem. Mater.* **2010,** *22,* 2790–2803
DOI:10.1021/cm903662a

CHEMISTRY OF MATERIALS
Article

Click Synthesis of Monolithic Silicon Carbide Aerogels from Polyacrylonitrile-Coated 3D Silica Networks

Nicholas Leventis,* Anand Sadekar, Naveen Chandrasekaran, and Chariklia Sotiriou-Leventis*

Department of Chemistry, Missouri University of Science and Technology (formerly University of Missouri−Rolla), Rolla, Missouri 65409

Received December 4, 2009. Revised Manuscript Received February 26, 2010

SiC retains high mechanical strength and oxidation stability at temperatures above 1500 °C, representing a viable alternative to silica, alumina, and carbon, which have been in use as catalyst supports for more than 60 years. Preparation of monolithic porous SiC is usually elaborate and porosities around 30% v/v are typically considered high. This report describes the synthesis of monolithic highly porous (70% v/v) SiC by carbothermal reduction (1200−1600 °C) of 3D sol−gel silica nanostructures (aerogels) conformally coated and cross-linked with polyacrylonitrile (PAN). Synthesis of PAN-cross-linked silica aerogels is carried out in one pot by simple mixing of the monomers, whereas conversion to SiC is carried out in a tube reactor by programmed heating. Intermediates after aromatization (225 °C in air) and carbonization (800 °C under Ar) were isolated and characterized for their chemical composition and materials properties. Data are interpreted mechanistically and were used iteratively for process optimization. Solids ^{29}Si NMR validates use of skeletal densities (by He pycnometry) for the quantification of the conversion of silica to SiC. Consistent with the topology of the carbothermal process, data support complete conversion of SiO_2 to SiC requiring a C:SiO_2 ratio higher than the stoichiometric one (=3). The morphology of the SiC network is invariant of the processing temperature between 1300 and 1600 °C, and hence it is advantageous to carry out the carbothemal process at higher temperatures where reactions run faster. Those samples are macroporous and consist of pure polycrystalline β-SiC (skeletal density: 3.20 g cm^{-3}) with surface areas in the range reported previously for biomorphic SiC (~20 m^2 g^{-1}). Although the micromorphology remains constant, the crystallite size of SiC increases with processing temperature (from 7.1 nm at 1300 °C to 16.5 nm at 1600 °C). Samples processed at 1200 °C are mesoporous and amorphous (by XRD), even though they consist of ~75% mol/mol SiC. The change in the morphology of SiC in the 1200−1300 °C range has been explained by a melting mechanism. This comprises the first report of using a polymer cross-linked aerogel for the synthesis of another porous material.

1. Introduction

Silicon carbide (SiC), a bioinert large band gap semiconductor (e.g., 2.36 and 3.05 eV for β- and α-SiC, respectively), combines hardness (9 to 9.5 on the Mohs scale), high thermal conductivity (120 W m^{-1} K^{-1}), low thermal expansion coefficient (4 × 10^{-6} °C^{1-}), good thermal shock resistance, and high mechanical strength/oxidation resistance at high temperatures (>1500°) and is a viable candidate for replacing silica, alumina, and carbon as supports for catalysts.[1,2]

Monolithic porous SiC can be prepared by sintering powders,[3,4] which are synthesized economically by carbothermal reduction of silica with carbon according to the old (1891) Acheson process (eq 1).[5]

$$SiO_2 + 3C \rightarrow SiC + 2CO \quad (1)$$

However, because of the high covalent character and strength of the sp^3−sp^3 C−Si bonds,[6] SiC itself is basically a nonsinterable material;[7] thereby, sintering is carried out reactively, usually with sintering aids (e.g., alumina, carbon). Oxidation bonding, wherein SiC compacts are heated at 1100−1500 °C in air, is a simple version of reactive sintering; porosities of up to 30% have been achieved by including sacrificial (oxidizable) graphite in the compacts and are considered high.[8]

*Corresponding author. Tel.: (573) 341-4391 (N.L.); (573) 341-4353 (C.S.-L.). E-mail: leventis@mst.edu (N.L.); cslevent@mst.edu (N.S.-L.).

(1) Birot, M.; Pillot, J.-P.; Dunogues, J. *Chem. Rev.* **1995**, *95*, 1443–1477.
(2) (a) Ledoux, M. J.; Pham-Huu, C. *CATTECH* **2001**, *5*, 226–246. (b) Ledoux, M. J.; Hantzer, S.; Pham-Huu, C.; Guille, J.; Desaneaux, M. P. *J. Catal.* **1988**, *114*, 176–185. (c) Moene, R.; Makkee, M.; Moulijn, J. A. *Appl. Catal., A* **1998**, *167*, 321–330.
(3) She, J. H.; Ohji, T. *J. Mater. Sci. Lett.* **2002**, *21*, 1833–1834.
(4) Oh, S. T.; Tajima, K.; Ando, M.; Ohji, T. *J. Am. Ceram. Soc.* **2000**, *83*, 1314–1316.
(5) (a) Meng, G. W.; Cui, Z.; Zhang, L. D.; Phillipp, F. *J. Cryst. Growth* **2000**, *209*, 801–806. (b) Klinger, N.; Strauss, E. L.; Komarek, K. L. *J. Am. Ceram. Soc.* **1966**, *49*, 369–375.
(6) Riedel, R.; Passing, G.; Schonfelder, H.; Brook, R. J. *Nature* **1992**, *355*, 714–717.
(7) Suwanmethanond, V.; Goo, E.; Liu, P. K. T.; Johnston, G.; Sahimi, M.; Tsotsis, T. T. *Ind. Eng. Chem. Res.* **2000**, *39*, 3264–3271.
(8) She, J. H.; Obji, T.; Kanzaki, S. J. *Eur. Ceram. Soc.* **2003**, *24*, 331–334.

Published on Web 03/23/2010

Alternatively, porous SiC is obtained by shape memory synthesis (SMS) wherein the product of eq 1 mimics the shape of the carbon source.[2] As will be discussed later, eq 1 is a complex process that starts with generation of SiO gas and CO at the SiO_2/C interface.[5] SiC is primarily the result of the gas−solid reaction between SiO(g) and C(s).[9] Thus, SMS of porous SiC was carried out initially with SiO(g) generated independently (e.g., by reacting Si and SiO_2) and porous carbon from various sources.[2] Because natural materials are renewable and relatively inexpensive, SMS conversion of biomorphic carbon (charcoal) to SiC that retains the hierarchical porous structure of the parent wood has been investigated extensively.[10] More economic alternatives include infiltration of charcoal with silica sol[11] and ultimately direct infiltration of the charcoal precursor (wood) with sodium silicate, thus eliminating even the pyrolysis step of converting wood to charcoal as that takes place in situ along the way of setting off the carbothermal process of eq 1.[12] Typical surface areas for biomorphic SiC are about 14 $m^2\ g^{-1}$. The methodology of using charcoal as a structure-directing agent has also been extended to artificial porous graphitic substrates.[13] The major drawback of using silica sols is the multi-infiltrations needed to bring the C:SiO_2 ratio at the stoichiometry of eq 1.

Carbon- or carbon-precursor-doped silica aerogels and xerogels have been employed as SiC precursors, not so much from a SMS perspective, but rather because of their high surface area that would increase the contact between the two solid-state reactants of eq 1.[14] In most instances, however, the resulting SiC is more whiskerlike than particulate. Whiskers are formed via a gas-phase reaction (eq 2) between the SiO(g) and CO(g) intermediates of eq 1[15−17]

$$SiO(g) + 3CO(g) \rightarrow SiC(s) + 2CO_2(g) \qquad (2)$$

It seems that the porous architecture of C-doped sol−gel networks facilitates retention and circulation of those gases long enough to promote eq 2 with loss of memory of the shape of the silicon and carbon sources. Formation of whiskers, however, represents a health hazard and therefore whiskers are undesirable.[2] Therefore, to take advantage, mimic, and maintain the monolithicity and microstructure of silica aerogels, there seems to be a need to encapsulate SiO_2 within the carbon precursor, ensuring that all SiO(g) generated at the interface of SiO_2 and C will pass necessarily through and react with carbon.

Coating silica with carbon was first reported by Koc.[18] In those experiments, fumed silica powder (Carbosil, 10 nm in diameter) was coated with pyrolytic carbon by multiple exposures to a static propylene atmosphere at 600 °C, followed by pyrolytic conversion to SiC at 1300−1600 °C under flowing Ar. Comparison of simple mixtures of Carbosil with carbon black revealed that more carbon remained unreacted in the mixed (∼10% w/w) rather than in the coated systems (5% w/w), suggesting a higher loss of SiO in the stream of flowing Ar from the mixtures. Furthermore, particle aggregation was higher in the mixed samples, while it was also observed that carbon in the carbon-coated samples prevented agglomeration and allowed production of fine powders (0.1−0.3 μm in diameter). More recently, Guo included Ni^{2+} in SiO_2/phenolic resin sols organizing the primary colloidal particles (10 nm) into large secondary grains (1000 nm) of phenolic resin with embedded silica particles.[19] The morphology of the resulting SiC changed from whiskerlike (in the absence of Ni^{2+}) to particulate. The disadvantage of this approach is the residual Ni in SiC that might limit its applications. No evidence for monolithicity was provided. Finally, Antonietti has reported on porous SiC monoliths prepared by infiltration of preformed macro/mesoporous (13 nm) SiO_2 monoliths with a THF solution of precondensed graphitic precursors (mesophased pitch).[20] Drying and pyrolysis at 1400 °C yielded SiC−SiO_2 composites that, after removal of SiO_2 with ammonium hydrogen fluoride, afforded SiC retaining the macro- and mesoporous character of the starting silica artifact. However, as in the case of filling voids in biomorphic carbon with silica, the stepwise preparation of macro/mesoporous silica, carbon infiltration, and final removal of unreacted SiO_2 may be time-consuming from an applications perspective.

Considered together, Koc's, Guo's, and Antonietti's studies point to the advantages of mimicking the structure of silica rather than that of carbon in the SMS of SiC. Those studies also suggest that for economy, methodology should be developed wherein a conformal coating of silica with the correct amount of the carbon precursor should be carried out cleanly in one pot together with the synthesis of the monolithic three-dimensional (3D) nanoparticulate silica framework; in essence, synthesis of porous SiC should be carried out quickly and reliably by reacting suitable precursors with minimum steps and byproducts. This is referred to as click chemistry.[21] The methodology for the synthesis of 3D silica networks coated conformally with polymers exists; the resulting monolithic 3D core−shell nanostructures are

(9) Matrin, H. P.; Ecke, R.; Muller, E. *J. Eur. Ceram. Soc.* **1998**, *18*, 1737–1742.
(10) Greil, P. *J. Eur. Ceram. Soc.* **2001**, *21*, 105–118.
(11) Qian, J.-M.; Wang, J.-P.; Qiao, G.-J.; Jin, Z.-H. *J. Eur. Ceram. Soc.* **2004**, *24*, 3251–3259.
(12) Vyshnyakova, K.; Yushin, G.; Pereselentseva, L.; Gogotsi, Y. *Int. J. Appl. Ceram. Technol.* **2006**, *3*, 485–490.
(13) Friedel, B.; Greulich-Weber, S. *Mater. Res. Soc. Symp. Proc.* **2008**, *1069*, D01–03.
(14) See for example: (a) Li, X.; Chen, X.; Song, H. *J. Mater. Sci.* **2009**, *44*, 4661–4667. (b) Lu, W.; Steigerwalt, E. S.; Moore, J. T.; Sullivan, L. M.; Collins, W. E.; Lukehart, C. M. *J. Nanosci. Nanotechnol.* **2004**, *4*, 803–808. (c) Li, X. K.; Liu, L.; Zhang, Y. X.; Shen, Sh. D.; Ge, Sh.; Ling, L. Ch. *Carbon* **2001**, *39*, 159–165. (d) Meng, G. W.; Zhang, L. D.; Qin, Y.; Feng, S. P.; Mo, C. M.; Li, H. J.; Zhang, S. Y. *J. Mater. Sci. Lett.* **1999**, *18*, 1255–1257. (e) Meng, G. W.; Zhang, L. D.; Mo, C. M.; Zhang, S. Y.; Qin, Y.; Feng, S. P.; Li, H. J. *J. Mater. Res.* **1988**, *13*, 2533–2538.
(15) Saito, M.; Nagashima, S.; Kato, A. *J. Mater. Sci. Lett.* **1992**, *11*, 373–376.
(16) Vyshnyakova, K. L.; Pereselentseva, L. N.; Cambaz, Z. N.; Yushin, G. N.; Gogotsi, Y. *Br. Ceram. Trans.* **2004**, *103*, 193–196.
(17) Vix-Guterl, C.; McEnaney, B.; Ehrburger, P. *J. Eur. Ceram. Soc.* **1999**, *19*, 427–432.
(18) Koc, R.; Cattamanchi, S. V. *J. Mater. Sci.* **1998**, *33*, 2537–2549.
(19) (a) Guo, X.-Y.; Jin, G.-Q. *J. Mater. Sci.* **2005**, *40*, 1301–1303. (b) Jin, G.-Q.; Guo, X.- Y. *Microporous Mesoporous Mater.* **2003**, *60*, 207–212.
(20) Sonnenburg, K.; Adelhelm, P.; Antonietti, M.; Smarsly, B.; Nöske, R.; Strauch, P. *Phys. Chem. Chem. Phys.* **2006**, *8*, 3561–3566.
(21) Nandivada, H.; Jiang, X.; J. Lahann, J. *Adv. Mater.* **2007**, *19*, 2197–2208.

Table 1. Formulations for One-Pot Synthesis of PAN-Cross-Linked Silica Aerogels

formulation	TMOS (mL) [mol]	Si-AIBN (mL) [mol][a]	CH_3OH (mL)	H_2O (mL)	AN (mL) [mol]
F-10-00	3.465 [0.0234]	11.5 [0.0130]	9.00	1.5	0.00 [0.0000]
F-10-30	3.465 [0.0234]	11.5 [0.0013]	6.30	1.5	2.70 [0.0407]
F-10-45	3.465 [0.0234]	11.5 [0.0013]	4.95	1.5	4.05 [0.0611]
F-10-60	3.465 [0.0234]	11.5 [0.0013]	3.60	1.5	5.40 [0.0814]
F-20-00	3.068 [0.0207]	23.0 [0.0026]	9.00	1.5	0.00 [0.0000]
F-20-30	3.068 [0.0207]	23.0 [0.0026]	6.30	1.5	2.70 [0.0407]
F-20-45	3.068 [0.0207]	23.0 [0.0026]	4.95	1.5	4.05 [0.0611]
F-20-60	3.068 [0.0207]	23.0 [0.0026]	3.60	1.5	5.40 [0.0814]
F-30-00	2.68 [0.0181]	34.5 [0.0039]	9.00	1.5	0.00 [0.0000]
F-30-30	2.68 [0.0181]	34.5 [0.0039]	6.30	1.5	2.70 [0.0407]
F-30-45	2.68 [0.0181]	34.5 [0.0039]	4.95	1.5	4.05 [0.0611]
F-30-60	2.68 [0.0181]	34.5 [0.0039]	3.60	1.5	5.40 [0.0814]

[a] Volume of a stock solution of Si-AIBN (0.1122 M) in THF.

referred to as polymer-cross-linked aerogels and are pursued for their impressive mechanical properties.[22] In this report, we describe a polymer cross-linked aerogel as the precursor for the synthesis of another porous material: silicon carbide aerogels. For this purpose, an aerogel is defined as an open nonfluid colloidal network or polymer network that is expanded throughout its whole volume by a gas, and is formed by the removal of all swelling agents from a gel without substantial volume reduction or network compaction. For the rationale of this definition, refer to the Supporting Information. Our cross-linking polymer of choice is polyacrylonitrile (PAN), which is used industrially for the pyrolytic manufacture of carbon fiber for automotive and aerospace applications.[23]

2. Experimental Section

Materials. All reagents and solvents were used as received unless noted otherwise. Anhydrous tetrahydrofuran (THF) was prepared by predrying HPLC-grade solvent over NaOH followed by distillation over $LiAlH_4$. Acrylonitrile (AN) was purchased from Aldrich Chemical Co. and washed with a 5% (w/w) aqueous sodium hydroxide solution to remove the inhibitor, followed by distillation under reduced pressure. Methanol and toluene were purchased from Fisher. The free radical inititator, Si-AIBN (4,4′-(diazene-1,2-diyl)bis-(4-cyano-*N*-(3-triethoxysilyl)propyl)pentanamide), was synthesized as described previously and was kept in dry THF (0.112 M) at 4 °C.[24]

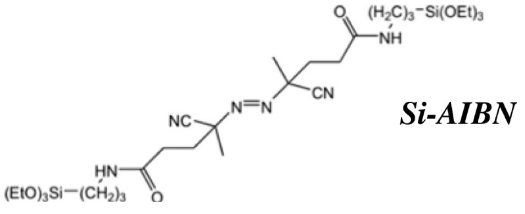

Si-AIBN

Preparation of Polyacrylonitrile (PAN)-Cross-Linked Silica Aerogels. The Si-AIBN stock solution was allowed to warm to room temperature, and an aliquot (23.0 mL, 0.0026 mol) was transferred into a round-bottom flask. The solvent was removed at room temperature under reduced pressure, and the resulting solid was dissolved in a mixture of methanol, tetramethylorthosilicate (TMOS) and AN. This is referred to as Solution A. A second solution (Solution B) was prepared by mixing methanol, AN, distilled water, and 80 μL of 14.8 N NH_4OH. The total amounts of methanol, TMOS and AN were varied as shown in Table 1 in order to (a) keep the total mol amount of silicon (1 mol from TMOS + 2 mol from Si-AIBN) constant in all samples, but vary the mol percent of silicon derived from Si-AIBN from 10 to 20 to 30% (the corresponding samples are referred to as F-10, F-20 and F-30, respectively, where "F" stands for "formulation"); and (b) vary the volume percent of AN to methanol + AN from 30 to 45 to 60% v/v. Thus, we ended up with three final samples for each Si-AIBN concentration. The predetermined amount of methanol and AN were divided equally between solution A and solution B. Solution B was added to solution A and this mixture comprises the sol. The sol was shaken well and poured into polypropylene molds (Wheaton polypropylene Omni-Vials, Part No. 225402, 1 cm in diameter). Sols gelled within 10−15 min. The resulting clear wet-gels were aged for 24 h at room temperature in their molds, exposed to UV light for 300 s (changing the angle of exposure frequently) using a UVitron International Intrelli-ray 600 shattered UV floodlight (600 W), heated at 55 °C for 12 h, solvent-exchanged with ethanol (3 times, 8 h per wash cycle to remove gelation water), and finally solvent-exchanged again with toluene (3 times, 8 h per wash cycle to remove free PAN from the pores). The resulting opaque-white alco-gels were dried into PAN-cross-linked aerogels in an autoclave with liquid CO_2 taken out at the end as a supercritical fluid (SCF). Alternatively, cross-linked wet-gels were dried directly from the molds under ambient pressure for 2−3 days without any further washes. The ambient drying approach simplifies the process tremendously, without any adverse effect on the quality of the final SiC monoliths. For comparison purposes, native samples (designated as F-10-00, F-20-00, and F-30-00) were also prepared by replacing AN with an equal volume of methanol (refer to Table 1).

Preparation of Silicon Carbide Aerogels from PAN-Cross-Linked Aerogels. PAN-cross-linked aerogels were initially aromatized by heating in air at 225 °C for 36 h. The color changed from white to brown. Subsequently, they were transferred to an MTI GSL1600X-80 tube furnace (tube and lining both of alumina 99.8% pure, 45 mm and 51 mm inner and outer diameters of lining, 72 and 80 mm inner and outer diameters

(22) (a) Leventis, N. *Acc. Chem. Res.* **2007**, *40*, 874–884. (b) Leventis, N.; Mulik, S.; Wang, X.; Dass, A.; Patil, V. U.; Sotiriou-Leventis, C.; Lu, H.; Churu, G.; Capecelatro, A. *J. Non-Cryst. Solids* **2008**, *354*, 632–644. (c) Leventis, N.; Sotiriou- Leventis, C.; Mulik, S.; Dass, A.; Schnobrich, J.; Hobbs, A.; Fabrizio, E. F.; Luo, H.; Churu, G.; Zhang, Y.; Lu, H. *J. Mater. Chem.* **2008**, *18*, 2475–2482. (d) Bertino, M. F.; Hund, J. F.; Zhang, G.; Sotiriou-Leventis, C.; Tokuhiro, A. T.; Leventis, N. *J. Sol−Gel Sci. Technol.* **2004**, *30*, 43–48. (e) Leventis, N.; Sotiriou-Leventis, C.; Zhang, G.; Rawashdeh, A.-M. M. *Nano Lett.* **2002**, *2*, 957–960.

(23) Morgan, P. *Carbon Fibers and Their Composites*; CRC Press: Boca Raton, FL, 2005.

(24) Mulik, S.; Sotiriou-Leventis, C.; Churu, G.; Lu, H.; Leventis, N. *Chem. Mater.* **2008**, *20*, 5035–5046.

of the tube, 457 mm heating zone) and heated further under flowing Ar (70 mL min^{-1}): The temperature of the tube furnace was first raised within 2 h from ambient to 300 °C and it was maintained at that level for 3 h. Subsequently, the temperature was raised further within 2 h to 800 °C, and maintained at that level for 3 h. Finally, the temperature was again raised within 5 h to the end carbothermal reaction temperature (from 1200 to 1600 °C) and it was maintained at that level for different time periods ranging from 36 to 140 h. At the end of that period, the temperature was lowered to 600 °C, flowing Ar was changed to flowing air, and excess of carbon was burned off by maintaining the temperature at that level for 5 h. Samples for analysis were removed at intermediate stages of the heating process (at 800 °C and at the end of the carbothermal process), by interrupting heating and by letting the tube furnace cool down to room temperature under flowing Ar.

Methods. Supercritical fluid CO_2 drying was conducted using an autoclave (SPI-DRY Jumbo Supercritical Point Drier, SPI Supplies, Inc., West Chester, PA). Bulk densities (ρ_b) were calculated from the weight and the physical dimensions of the samples. Skeletal densities (ρ_s) were determined using helium pycnometry with a Micromeritics AcuuPyc II 1340 instrument. Porosities were determined from the ρ_b and ρ_s values. Surface areas (σ) were measured by nitrogen adsorption/desorption porosimetry using a Micromeritics ASAP 2020 surface area and pore distribution analyzer. Samples for surface area and skeletal density determinations were outgassed for 24 h at 80 °C under a vacuum before analysis. Average pore diameters were determined by the $4 \times V_{total}/\sigma$ method, where V_{total} is the total pore volume per gram of sample. V_{total} was calculated from either the single highest volume of N_2 adsorbed along the adsorption isotherm or the relationship $V_{total} = (1/\rho_b) - (1/\rho_s)$. The single-point N_2 adsorption method tends to underestimate V_{total} significantly when macropores are involved.[25] The discrepancy between average pore diameters calculated by the two methods was taken as an indication of macroporosity. In that case, discussion of average pore diameters is based on values calculated using $V_{total} = (1/\rho_b) - (1/\rho_s)$. Samples of cross-linked silica aerogels, silicon carbide, and intermediates were characterized by solid ^{13}C and ^{29}Si NMR spectroscopy using one-pulse sequence with magic angle spinning (at 7 kHz). Samples up to the point of aromatization (heated at 225 °C) were characterized by ^{13}C CPMAS-TOSS pulse sequence solids NMR with broadband proton decoupling and magic angle spinning (at 5 kHz). Samples after carbonization (800 °C) contain no hydrogen and were characterized by one-pulse sequence and magic angle spinning (at 7 kHz). All samples were ground to fine powder and packed into 7 mm rotors. A Bruker Avance 300 wide bore NMR spectrometer equipped with a 7 mm CPMAS probe was used. The operating frequency for ^{13}C and ^{29}Si was 75.483 and 59.624 MHz, respectively. ^{13}C NMR spectra were referenced externally to glycine (carbonyl carbon at 176.03 ppm). ^{29}Si NMR spectra were referenced externally to neat tetramethylsilane (TMS, 0 ppm). Modulated differential scanning calorimetry (MDSC) was conducted in air with a TA Instrument Model 2920 apparatus at a heating rate of 10 °C min^{-1}. SiC samples at the end of processing were characterized by X-ray diffraction. Those experiments were performed with powders of the corresponding materials using a Scintag 2000 diffractometer with Cu Kα radiation and a proportional counter detector equipped with a flat graphite monochromator. Structural information for silicon carbide was obtained using the ICSD database version 2.01. The crystallite size was estimated with the Jade software (version 5.0, Materials Data, Inc.) using Scherrer's equation. A Gaussian correction for instrumental broadening was applied utilizing NIST SRM 660a LaB6 for the determination of the instrumental broadening. Scanning electron microscopy (SEM) was conducted with samples coated with Au−Pd using a Hitachi S-4700 field emission microscope.

Scheme 1. Flowchart for the Synthesis and Characterization of SiC Aerogels

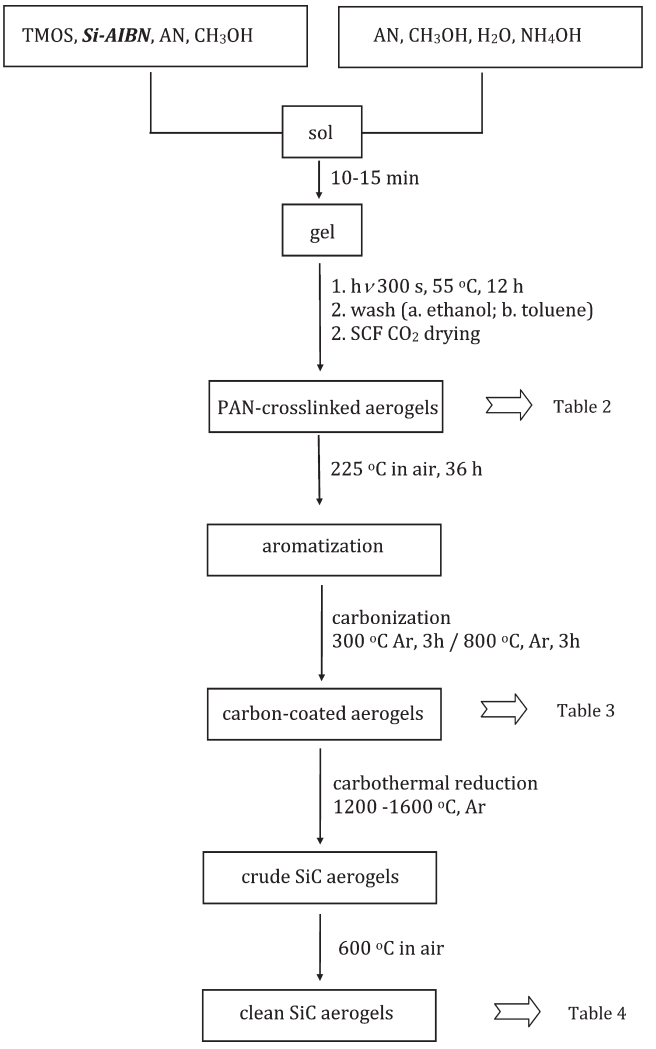

Determination of Organic Matter in Native Samples. The incorporation of Si-AIBN in the silica (TMOS) framework was evaluated by correlating the amount of organic matter in native F-10-00, F-20-00, and F-30-00 aerogels with the concentration of Si-AIBN in their sol. The amount of organic matter was determined gravimetrically before and after heating native samples at 600 °C in air.

Determination of the PAN Content in Selective PAN-Cross-Linked Samples. The same process as above was applied to F-20-45 samples. The weight percent of PAN thus was calculated by factoring in the ratio of SiO_2 and of the organic matter originating from Si-AIBN.

Determination of C:SiO_2 Ratio Available for the Carbothermal Reduction. This ratio was determined gravimetrically, by recovering samples at 800 °C during the carbothermal process. The samples were weighed, then heated again at 600 °C in air to burn off remaining carbon.

Determination of the Conversion of SiO_2 to SiC. PAN-crosslinked samples with known content of silica were weighed before and after processing at different carbothermal temperatures

(25) Fricke, J.; Reichenauer, G. *J. Non-Cryst. Solids* **1987**, *95&96*, 1135–1142.

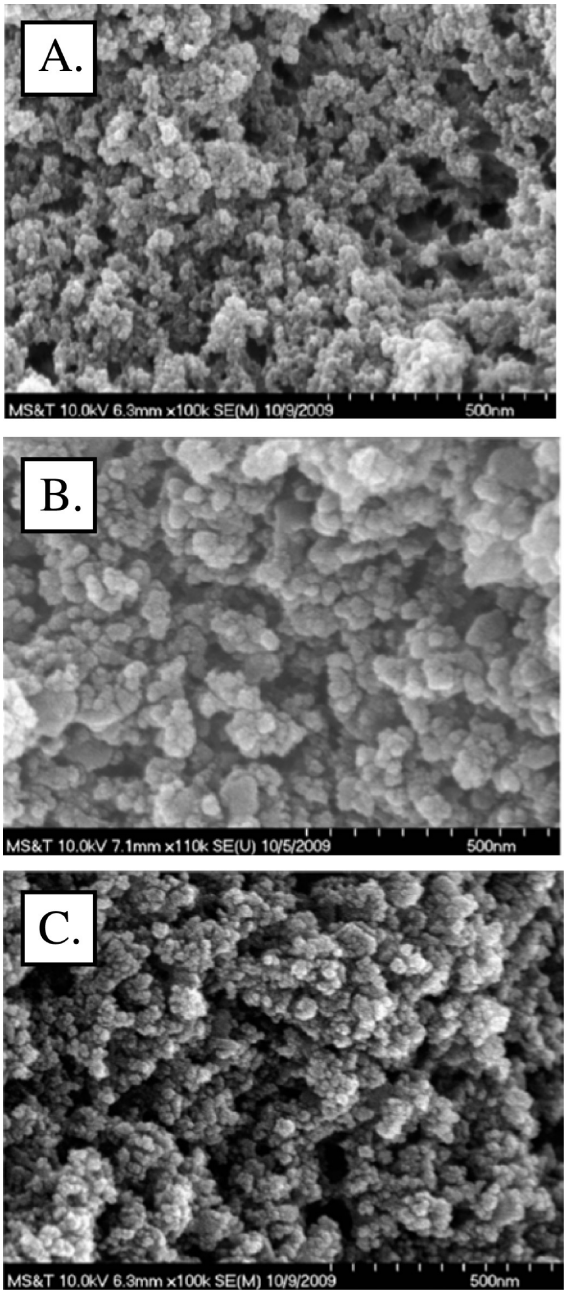

Figure 1. Scanning electron micrographs (SEM) of PAN-cross-linked F-20-45 samples: (A) as-prepared; (B) after heating at 225 °C in air for 36 h (aromatization); and (C) after additional heating first at 300 °C for 3 h and at 800 °C under argon for 3 h (carbonization).

followed by removal of residual carbon at 600 °C in air. The efficiency of the carbothermal reduction of SiO_2 was determined by correlating the initial amount of silica to the final weight of SiC.

3. Results

3.1. General. Scheme 1 summarizes the overall process for the synthesis and conversion of PAN-coated silica aerogels to porous monolithic SiC. The sequence starts with the one-pot synthesis of PAN-coated silica wet-gels that are dried to PAN-cross-linked silica aerogels with SCF CO_2. The PAN coating is aromatized at 225 °C in air, and subsequently samples are placed in a tube furnace and heated stepwise under flowing Ar to a range of terminal temperatures from 1200 to 1600 °C. Unreacted carbon is removed at 600 °C in air. Although the entire process can be carried out continuously, several runs were interrupted at various intermediate stages and samples were analyzed in order to identify the controlling parameters and optimize the synthetic conditions for complete conversion of SiO_2 to monolithic SiC. Specifically, samples were also analyzed after aromatization at 225 °C, after carbonization at 800 °C, and before removal of unreacted carbon. Results are summarized in Tables 2−5. Alternatively, the entire process is shortened by eliminating the SCF CO_2 drying step; it was found (Table 6) that these new SiC samples were identical to those received by the lengthier process.

3.2. Synthesis of PAN-Cross-Linked Aerogels. Mesoporous monolithic silica was coated (cross-linked) with PAN in one pot through surface initiated free-radical polymerization (SIP) of the monomer (AN) according to eq 3.

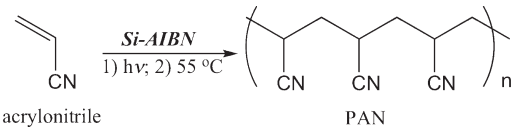

(3)

Si-AIBN, a bidentate free-radical initiator, was designed specifically to attach itself on silica at both ends so that the polymer produced by thermal or photochemical cleavage of the central −N=N− group remains surface-bound, rendering post-cross-linking washes unnecessary.[24] Nevertheless, it was found that some free PAN is still produced in the pores, presumably by an unidentified radical-transfer mechanism, and although its removal is not necessary (see section 4), post-cross-linking washes were conducted anyway to confirm and understand the topology of the processes taking place at the surface of silica during its conversion to SiC. It is further noted that up to now, cross-linking reagents for this class of materials have been introduced by time-consuming solvent exchanges after gelation;[2] here, however, because gelation of TMOS (a nucleophilic substitution process) does not interfere with the free-radical cross-linking reagents, both gelation and cross-linking chemistries have been included together in the sol, rendering postgelation (precross-linking) solvent exchanges unnecessary. Gelation takes place at room temperature, whereas cross-linking is triggered postgelation during aging in one pot (Scheme 1).

The amount of AN in the sol is related to the amount of carbon produced on the surface of silica during the carbonization process (see below). On the other hand, because surface-confined PAN is expected to be capped by two initiator fragments, the mol ratio of Si-AIBN:AN in the sol controls the length of the interparticle PAN tethers. By varying the Si-AIBN:total Si (TMOS + Si-AIBN) mol ratio (the total mol of Si remaining constant) from 0.1 to 0.2 to 0.3, it was found gravimetrically that the amount of Si-AIBN-related organic matter in the native (non-cross-linked) samples varied linearly (R = 0.99) from 15.9 to 21.8 to 26.2% w/w, respectively, signifying that all Si-AIBN was incorporated in the silica structure. The complete characterization data for the native and PAN-cross-linked samples are summarized in Table 2.

Table 2. Selected Properties of PAN-Cross-Linked Silica Aerogels

sample	diameter (cm)[a]	percent shrinkage (%)[b]	bulk density, ρ_b (g cm^{-3})	skeletal density, ρ_s (g cm^{-3})[c]	porosity, Π (% void space)	BET surface area, σ (m^2 g^{-1})	average pore diameter (nm)[d]	particle radius, r (nm)[e]
F-10-00	0.925 ± 0.003	5.0	0.177 ± 0.004	1.887 ± 0.006	90	681	8.5 [10.0]	2.2
F-10-30	0.923 ± 0.001	7.7	0.329 ± 0.011	1.498 ± 0.003	78	322	14.1 [14.5]	6.2
F-10-45	0.938 ± 0.003	6.2	0.426 ± 0.004	1.462 ± 0.003	71	206	13.2 [20.1]	10.0
F-10-60	0.945 ± 0.007	5.5	0.475 ± 0.007	1.478 ± 0.002	68	228	15.6 [17.6]	8.9
F-20-00	0.920 ± 0.005	8.0	0.190 ± 0.002	1.798 ± 0.004	89	647	14.28 [9.9]	2.2
F-20-30	0.936 ± 0.004	6.4	0.360 ± 0.005	1.435 ± 0.009	75	275	15.0 [15.6]	7.6
F-20-45	0.948 ± 0.003	5.2	0.414 ± 0.004	$1.45_8 \pm 0.01_0$	72	157	23.7 [26.7]	13.1
F-20-60	0.947 ± 0.004	5.3	0.467 ± 0.004	1.423 ± 0.007	67	144	13.9 [26.6]	14.6
F-30-00	0.922 ± 0.003	7.8	0.198 ± 0.003	1.705 ± 0.002	88	643	9.5 [9.4]	2.7
F-30-30	0.925 ± 0.002	7.5	0.378 ± 0.003	1.428 ± 0.009	74	195	14.3 [21.5]	10.8
F-30-45	0.931 ± 0.002	6.9	0.470 ± 0.002	1.448 ± 0.007	68	147	15.6 [26.6]	14.1
F-30-60	0.950 ± 0.001	5.0	0.473 ± 0.003	$1.42_3 \pm 0.08_9$	67	151	32.4 [25.1]	13.9

[a] Average of 5 samples. [b] Relative to the molds (1 cm diameter). [c] One sample, average of 50 measurements. [d] By the $4V_{total}/\sigma$ method. For the first number, V_{total} was calculated by the single-point adsorption method; for the number in brackets, V_{total} was calculated via $V_{total} = (1/\rho_b) - (1/\rho_s)$. [e] Calculated via $r = 3/\rho_s\sigma$.

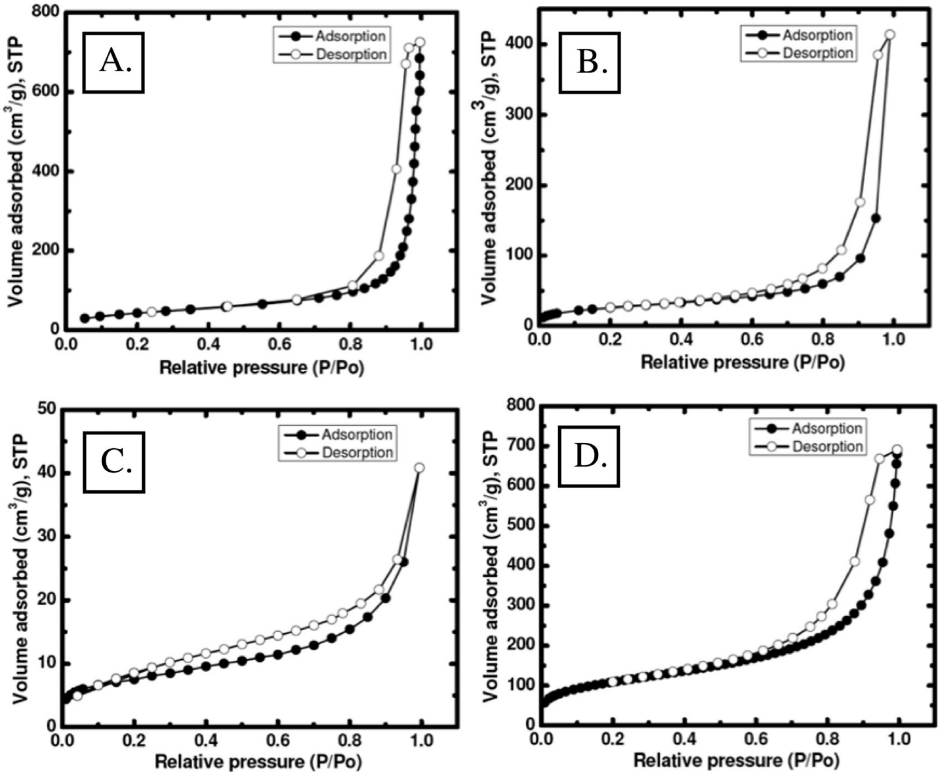

Figure 2. Nitrogen sorption isotherms of F-20-45 samples: (A) as-prepared; (B) after aromatization and carbonization (heating at 225 °C in air, followed by heating at 800 °C under Ar); (C) after carbothermal treatment at 1200 °C for 72 h under Ar, followed by oxidative cleaning at 600 °C in air; and (D) after carbothermal treatment at 1600 °C for 72 h under Ar, followed by oxidative cleaning at 600 °C in air.

PAN-cross-linking under our conditions causes a density increase relative to the native samples by a factor up to 2.5 (typical for these types of materials).[22] Generally, cross-linked samples shrink less relative to the molds in comparison with the native samples. Microscopically, cross-linked samples (Figure 1A) look similar to their native counterparts,[24] consistent with a tight conformal polymer coating of the skeletal silica nanoparticles. N_2 adsorption isotherms are Type IV, showing the characteristic desorption hysteresis of mesoporous materials (Figure 2A). The BET surface area, σ, has been decreased relative to the area of the native samples (Table 2) indicating that the polymer has smoothed out the surface of the secondary particles blocking access for N_2 to the smaller crevices on the skeletal framework,[24] and consistent with the average pore diameter increase reported in Table 2. (It is noted that average pore diameters calculated either from the single-point total pore volume (V_{total}) obtained from the adsorption isotherm, or via the $V_{total} = 1/\rho_b - 1/\rho_s$ method are close numerically and both within the mesoporous range (2−50 nm), further supporting the mesoporous nature of those samples.) The porosity, Π, as % v/v of empty space, has been decreased from ∼90% in the native samples to ∼70% in the cross-linked samples, consistent with the particle size increase (calculated via radius $r = 3/\rho_s\sigma$,

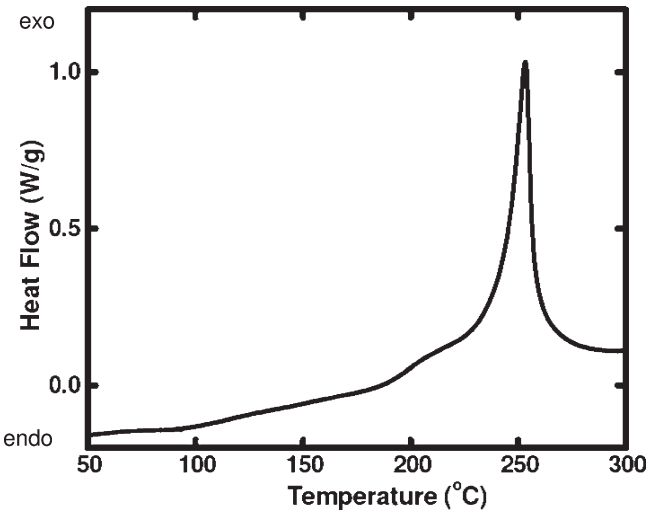

Figure 3. Differential scanning calorimetry (DSC) in air of a F-10-60 aerogel (heating rate: 10 °C min^{-1}).

Table 2) brought about by the conformal polymer coating.

3.3. Aromatization of PAN-Cross-Linked Aerogels. Conversion of PAN to carbon requires prior aromatization, which is typically induced oxidatively by heating the polymer between 270 and 300 °C in air (eq 4).[24,26,27]

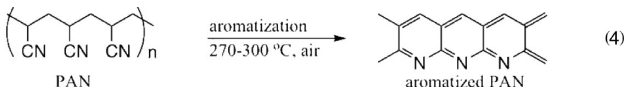

(4)

Indeed, direct heating of PAN-cross-linked aerogels at 800 °C in argon causes decomposition of the polymer and complete loss of the organic matter. Heating PAN-cross-linked samples in air shows a sharp exotherm with a peak at 253 °C (by DSC; Figure 3). Aromatization (followed by ^{13}C NMR, Figure 4) takes place at both sides of the exotherm, albeit more slowly at the low temperature end (225 °C versus 300 °C, refer to Figure 4). However, processing PAN-cross-linked silica aerogel monoliths at 300 °C tends to break them into small pieces, presumably because of the stresses on the silica framework created by the structural rearrangement of the polymer during its aromatization. On the other hand, a combination of conditions expected to produce shorter polymer chains (higher Si-AIBN concentrations: F-20 and F-30 formulations) with lower aromatization temperatures seem to yield monoliths with 100% success rate. Microscopically, those samples look quite similar to their parent PAN-cross-linked aerogels (Figure 1B). Therefore, for further processing, we opted to heat samples for longer time periods (36 h) at 225 °C (Scheme 1). The incomplete aromatization of PAN under those conditions (see spectrum in Figure 4 labeled "225 °C in air") necessitated determination of the C:SiO_2 mol ratio produced after carbonization as a function of the initial formulation of the PAN-cross-linked samples.

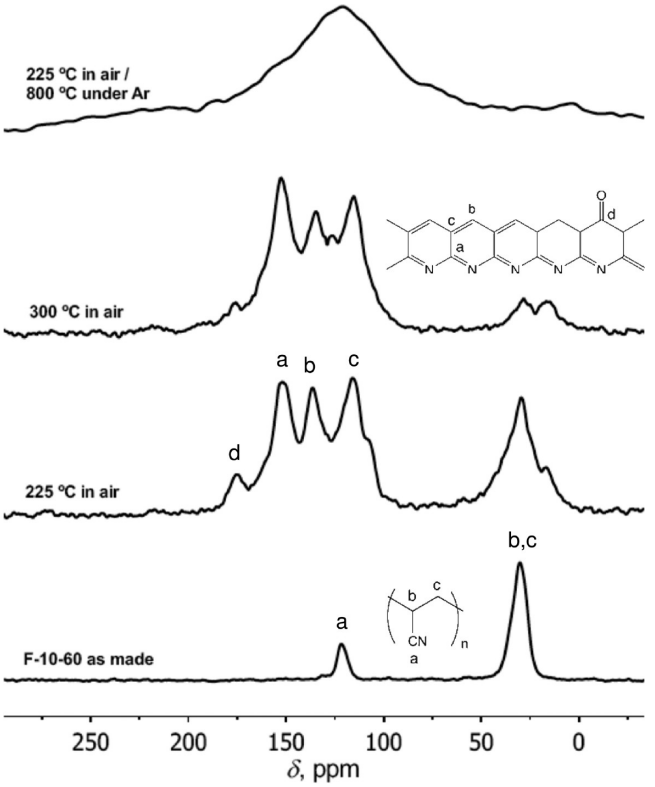

Figure 4. Solids CPMAS ^{13}C NMR data of F-10-60 aerogels processed under the conditions indicated. Peak assignment according to ref 27, confirmed by simulations.

3.4. Carbonization of Aromatized PAN-Cross-Linked Aerogels. Aromatized PAN-cross-linked aerogels are converted to SiC by heating in the 1200−1600 °C range under Ar. As confirmed by ^{13}C NMR (Figure 4), at around 800 °C aromatized PAN is converted to carbon (eq 5).[24,26] Aromatized samples heated at just 800 °C

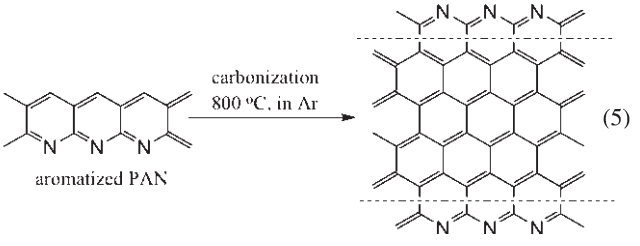

(5)

allow correlation of the initial synthetic conditions to the C:SiO_2 mol ratio. The complete analysis of the carbonized samples is summarized in Table 3. Carbonization causes additional shrinkage (12−13%) relative to the parent PAN-cross-linked aerogel precursors, but samples retain their shape and micromorphology (by SEM, Figure 1C). N_2 adsorption isotherms (Figure 2B) show signs of macroporosity (lower total volume of N_2 adsorbed, lack of saturation, most of the increase in the volume adsorbed is observed above 90% of relative pressure), and pore diameters calculated via the $V_{total}/4\sigma$ method using V_{total} obtained by the single point versus the $V_{total} = 1/\rho_b - 1/\rho_s$ method do not match, the latter being significantly larger, in fact in the range of macropores (> 50 nm, see Table 3). The BET surface area after carbonization is also

(26) Rahaman, M. S. A.; Ismail, A. F.; Mustafa, A. *Polym. Degrad. Stab.* **2007**, *92*, 1421–1432.
(27) Usami, T.; Itoh, T.; Ohtani, H.; Tsuge, S. *Macromolecules* **1990**, *23*, 2460–2465.

Table 3. Characterization of PAN-Cross-Linked Silica Aerogels after Pyrolysis at 800 °C

sample	diameter (cm)[a]	percent shrinkage (%)[a,b]	bulk density, ρ_b (g cm^{-3})[a]	skeletal density, ρ_s (g cm^{-3})[c]	porosity, Π (% void space)	BET surface area, σ (m^2 g^{-1})	average pore diameter (nm)[d]	particle radius, r (nm)[e]	C:SiO$_2$ (mol/mol)
F-10-30	0.823	13	0.290	$2.18_7 \pm 0.02_4$	86	124	24.2 [60.8]	11.0	2.55
F-10-45	0.832	12	0.333	2.118 ± 0.003	84	93	13.8 [76.1]	15.1	4.65
F-10-60	0.845	11	0.357	2.149 ± 0.006	83	79	16.5 [90.5]	17.6	8.85
F-20-30	0.849	13	0.276	$2.13_4 \pm 0.04_2$	87	96	13.5 [76.9]	14.5	4.36
F-20-45	0.834	12	0.365	$2.17_8 \pm 0.01_1$	83	94	12.8 [76.7]	14.6	7.08
F-20-60	0.834	12	0.410	2.140 ± 0.008	80	74	18.0 [93.2]	18.9	7.66
F-30-30	0.843	13	0.321	$2.17_8 \pm 0.01_1$	85	99	17.1 [74.9]	13.9	4.36
F-30-45	0.822	13	0.396	2.156 ± 0.009	81	79	14.2 [88.1]	17.4	6.85
F-30-60	0.840	12	0.495	2.140 ± 0.007	77	69	18.4 [90.0]	20.3	9.49

[a] Single sample. [b] Relative to the PAN-cross-linked aerogels. [c] Single sample, average of 50 measurements. [d] By the $4V_{total}/\sigma$ method. For the first number, V_{total} was calculated by the single-point adsorption method; for the number in brackets, V_{total} was calculated via $V_{total} = (1/\rho_b) - (1/\rho_s)$. [e] Calculated via $r = 3/\rho_s\sigma$.

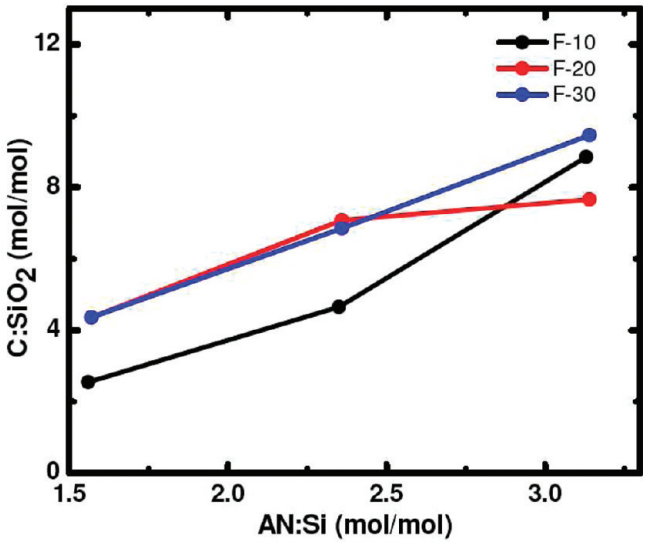

Figure 5. Correlation of the C:SiO$_2$ mol ratio after aromatization and carbonization with the initial AN:total Si mol ratio in the formulations listed in Table 1 (total Si: TMOS + 2Si-AIBN).

significantly lower than that of the parent PAN-cross-linked samples (69−124 m^2 g^{-1} versus 140−320 m^2 g^{-1}, respectively; compare Tables 2 and 3). Consequently, the particle size of the carbonized samples is calculated larger than that of the parent PAN-cross-linked aerogels (11.0−20.3 nm versus 6.2−14.6 nm, respectively). The porosimetry data considered together with SEM are consistent with a rather compact C-coating blocking access to the underlying silica network. The C:SiO$_2$ ratio (included in Table 3) was determined gravimetrically and increase together with the AN:SiO$_2$ mol ratio in the original sol (Figure 5) from substoichiometric (e.g., 2.55 for the F-10-30 formulation) to a little over the stoichiometric (~4.4 for the F-10-45, F-20-30, and F-30-30 formulations) to over twice the stoichiometric ratio of eq 1 (samples F-10-60, F-20-45, F-10-50, F-30-45, and F-30-60). Because F-10 samples tend to break in pieces after aromatization, and because F-30 samples use a larger amount of Si-AIBN unnecessarily, only F-20-30 and F-20-45 samples were considered for further processing.

3.5. Conversion of Aromatized PAN-Cross-Linked Aerogels to SiC. Thermodynamically, eq 1 and the associated elementary processes (see Discussion below), depend on the partial pressure of CO. Thus, while under atmospheric pressure, generation of SiC requires temperatures above ~1754 °C,[18] thermobarometric analysis under dynamic vacuum (1×10^{-2} Pa) has shown that carbothermal reduction of silica xerogels impregnated with saccharose can start at 1100 °C.[28] Similarly, under dynamic Ar-flow (1 kPa of total SiO and CO pressure) SiC reportedly started forming from 1220 °C.[17] For our carbothermal work, we opted for flowing Ar, and focused on materials prepared in the 1200−1600 °C range. Materials characterization data for selected samples clean of unreacted carbon, namely F-20-30 and F-20-45, processed at different temperatures for different times are summarized in Table 4. ^{29}Si NMR has been a reliable tool for differentiating silicon from SiC (−13 ppm) and SiO$_2$ (−105 ppm), even in amorphous phases. Indeed, although according to XRD data (Figure 6) cubic (3C of β-) SiC starts showing up above 1300 °C, ^{29}Si NMR (Figure 7) clearly shows a 3.8:1 mol/mol ratio of SiC:SiO$_2$ at 1200 °C. After pyrolysis at 1300 °C the relative amount of SiC increases (the SiC:SiO$_2$ mol ratio reaches 6.6), and after pyrolysis at 1600 °C polycrystalline SiC (mostly 3C with a small amount of 6H) is the only detectable Si-phase. Importantly, using literature density values for silicon carbide (3.20 g cm^{-3}) and sintered amorphous silica (2.1 g cm^{-3}),[29,30] the SiC:SiO$_2$ mol ratios determined by ^{29}Si NMR can be converted to the skeletal densities expected of the final C-clean samples. Thus, it is calculated from the data of spectra B and C in Figure 7 that the expected skeletal densities (ρ_s) of terminal free-of-carbon F-20-30 samples should be 2.969 and 3.054 g cm^{-3} for samples pyrolyzed at 1200 and 1300 °C, respectively. Those values agree well with the experimental ρ_s data (2.968 and 3.014 g cm^{-3}, respectively, refer to Table 4) suggesting and validating use of ρ_s data for assessing purity of the SiC. Indeed, F-20-45 samples processed at 1600 °C show only the ^{29}Si resonance peak of SiC (Figure 7D) and their skeletal density is that of pure SiC (Table 4).

(28) Zheng, Y.; Zheng, Y.; Wang, R.; Wei, K. *J. Mater. Sci.* **2008**, *43*, 5331–5335.
(29) Scherer, G. W.; Calas, S.; Sempere, R. *J. Non.-Cryst. Solids* **1998**, *240*, 118–130.
(30) Emmerling, A.; Lenhard, W.; Fricke, J.; Van de Vorst, G. A. L. *J. Sol−Gel Sci. Technol.* **1997**, *8*, 837–842.

Table 4. Characterization of SiC Aerogels Prepared under Different Conditions

sample (°C) [h]	diameter (cm)[a]	shrinkage (%)[a,b]	bulk density, ρ_b (g cm^{-3})[a]	skeletal density, ρ_s (g cm^{-3})[c]	porosity, Π (% void space)	BET surface area, σ (m^2 g^{-1})	average pore diameter (nm)[d]	particle radius, r (nm)[e]	crystallite size (nm)[f]
				F-20-30 (C:SiO_2 = 4.36 mol/mol)					
1200 [36]	0.487	48	0.623	$2.96_8 \pm 0.02_4$	81	221	14.6 [23.0]	4.6	[g]
1200 [72]	0.555	41	0.533	$2.94_4 \pm 0.01_7$	78	198	15.6 [31.0]	5.1	[g]
1300 [36]	0.536	43	0.591	$3.01_4 \pm 0.02_8$	79	108	20.9 [51.4]	9.4	7.5 ± 0.9
1300 [72]	0.540	42	0.526	$3.07_8 \pm 0.01_0$	76	42	21.3 [150]	23.2	[h]
1400 [36]	0.578	39	0.503	$3.02_1 \pm 0.01_9$	75	16	21.2 [415]	61.9	14.6 ± 0.3
1400 [72]	0.565	40	0.515	$3.11_8 \pm 0.01_3$	74	18	15.4 [360]	53.5	[h]
				F-20-45 (C:SiO_2 = 7.08 mol/mol)					
1200 [36]	0.578	30	0.410	2.919 ± 0.006	71	394	17.6 [21.3]	2.6	[g]
1200 [72]	0.567	40	0.401	$2.92_8 \pm 0.03_2$	71	381	16.1 [22.6]	2.7	[g]
1200 [110]	0.563	40	0.447	$2.91_7 \pm 0.09_9$	71	370	10.8 [20.5]	2.8	[g]
1200 [140]	0.583	38	0.441	$2.9_3 \pm 0.1_2$	69	385	9.4 [20.0]	2.7	[g]
1300 [36]	0.589	38	0.473	$3.08_8 \pm 0.01_4$	71	53	22.7 [135]	18.3	[h]
1300 [72]	0.612	35	0.446	$3.17_0 \pm 0.02_8$	72	22	18.1 [350]	43.0	7.1 ± 0.8
1400 [72]	0.598	37	0.481	$3.15_3 \pm 0.05_4$	72	20	12.5 [353]	47.6	14.9 ± 0.9
1500 [72]	0.590	38	0.430	$3.19_0 \pm 0.03_3$	70	16	16.9 [502]	58.8	16.6 ± 0.8
1600 [72]	0.579	39	0.482	$3.20_0 \pm 0.04_3$	75	13	21.7 [542]	72.1	16.5 ± 1.3

[a] Analysis of a single sample for each formulation. [b] Shrinkage relative to the diameter of the PAN-cross-linked aerogels. [c] Analysis of a single sample, average of 50 measurements. [d] By the $4V_{total}/\sigma$ method. For the first number, V_{total} was calculated by the single-point adsorption method; for the number in brackets, V_{total} was calculated via $V_{total} = (1/\rho_b) - (1/\rho_s)$. [e] Calculated via $r = 3/\rho_s\sigma$. [f] By XRD using the Scherrer equation; averages from the values obtained from the (111), (220), and (311) reflections. [g] Amorphous. [h] Not determined.

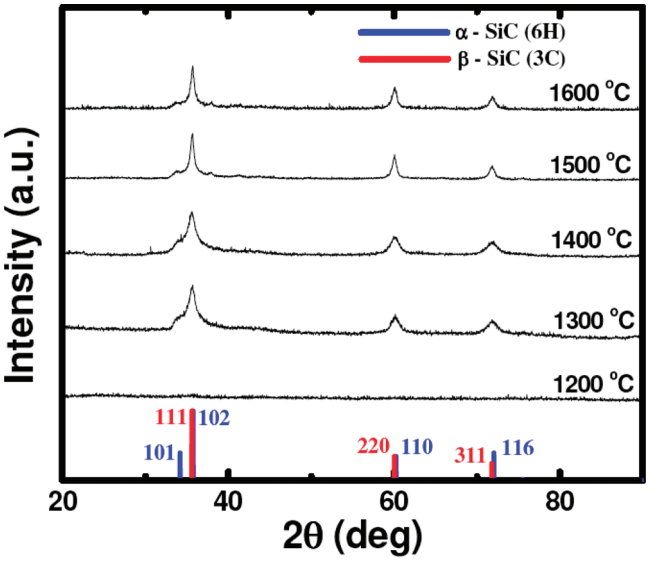

Figure 6. XRD data for F-20-45 samples after carbothermal treatment under flowing Ar for 72 h at the temperatures indicated, followed by oxidative removal of unreacted carbon at 600 °C in air. Using methods outlined in the Experimental Section and based on the relative intensities of the (101) reflection of α-SiC and the subsequent overlapping reflections of α- and β-SiC, it is concluded that the main product at all temperatures is β-SiC.

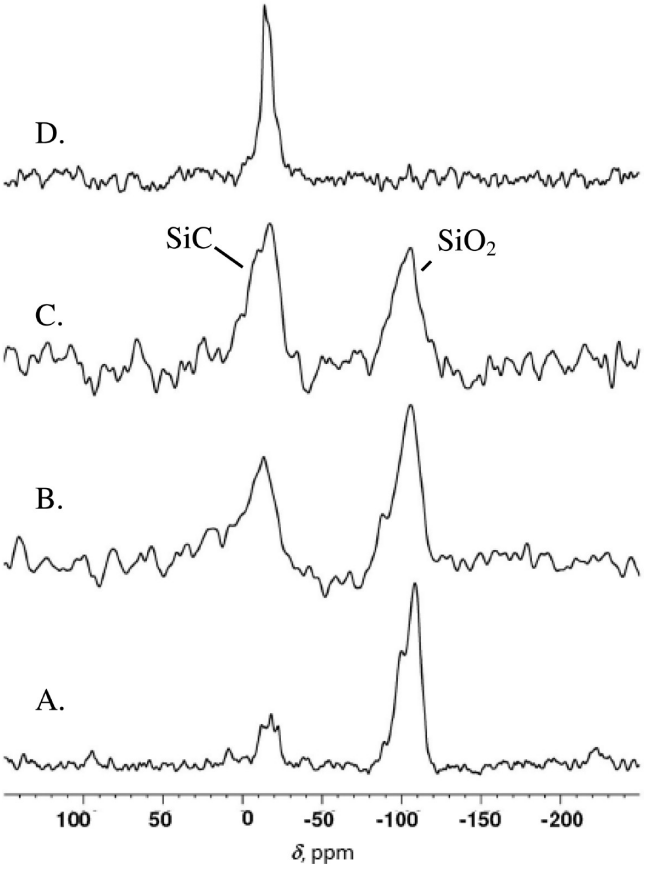

Figure 7. Solids ^{29}Si NMR of: (A) 1:1 mol/mol mixture of commercial SiC and silica (calibration sample used for integration of B and C); (B) F-20-30 sample treated carbothermally at 1200 °C for 36 h followed by treatment at 600 °C in air; (C) F-20-30 sample treated carbothermally at 1300 °C for 36 h, followed by treatment at 600 °C in air; and (D) F-20-45 sample treated carbothermally at 1600 °C followed by treatment at 600 °C in air.

Overall, Table 4 shows that pyrolytically F-20−30 and F-20−45 samples behave quite similarly. For example, above 1400 °C, there is no significant difference either in their degree of shrinkage or their bulk densities; below 1400 °C, all samples processed for shorter time periods (36 h rather than 72 h) seem to contain more unreacted silica, as reflected by consistently lower ρ_s values. There are some subtle differences, however. At lower temperatures (1200 and 1300 °C) F-20-30 samples shrink more (43−48%) than their more carbon-rich F-20-45 counterparts (30−40%) and that difference is reflected directly into higher bulk densities (~0.60 g cm^{-3} versus ~0.45 g cm^{-3}, respectively). To explain these shrinkage and density differences it is suggested that although all carbothermal reduction temperatures used are well

Table 5. Conversion Efficiency of SiO_2 in PAN-Cross-Linked F-20-45 samples into SiC

processing at °C[a]	sample (g)	weight of SiO_2 (g)[b]	expected SiC (g)	"crude" [c] material (g)	calculated weight of pure SiC (g)[d]	SiC yield (% w/w)
1300/600	1.1987	0.3836	0.2578	0.2581	0.2544	98.7
1400/600	1.1677	0.3737	0.2511	0.2570	0.2358	93.9
1500/600	1.1498	0.3679	0.2473	0.2511	0.2500	101.1
1600/600	1.1504	0.3681	0.2474	0.2384	0.2384	96.4

[a] Processing time at the two temperatures: 72 h/5 h, as described in the Experimental Section. [b] Based on 32% w/w silica (see text). [c] "Crude" means uncorrected for the amount of SiO_2 contained. [d] Calculated by considering the SiC/SiO_2 mol/mol ratio in the samples as dictated by the skeletal density data (Table 4).

above the typical sintering temperatures of sol−gel silica (~1050 °C),[29,30] nevertheless the thicker C-coating of the F-20−45 samples prevents that process more effectively, in agreement with Koc's report on reduced agglomeration of carbon-coated Carbosil, as summarized in the Introduction.[18] The tendency of F-20-30 samples to shrink more and contain slightly more unreacted silica, as well as the relative ease by which more C-rich F-20-45 samples are converted to pure SiC (their ρ_s values become within error equal to that of pure SiC even at 1300 °C for 72 h of processing), directed our further attention to the latter.

As established gravimetrically (see Experimental Section) PAN-cross-linked F-20−45 samples consist of 32% w/w SiO_2, 8.9% w/w Si-AIBN related organic matter and 59% w/w PAN. In turn, according to the data of Table 5, the SiO_2-to-SiC conversion efficiency for samples processed between 1300 and 1600 °C can be considered, within error, as 100% complete.

Spatial information for the location of the carbothermal reduction is obtained by SEM before and after oxidative removal of unreacted carbon. Before treatment at 600 °C in air, F-20-45 samples heated anywhere between 1300 and 1600 °C look superficially similar to their carbonized precursors recovered at 800 °C (compare the left column of Figure 8 to Figure 1C). Upon closer examination of Figure 8 though, larger particles (pointed at by circles and arrows) are discernible through the top layer. After treatment at 600 °C in air, the debris is removed, confirming that it consists of unreacted carbon. All samples having been heated carbothermally for 72 h between 1300 and 1600 °C look identical to one another (Figure 8, right column). No whiskerlike material is seen in the pores. All samples are macroporous (confirmed by N_2 adsorption, see Figure 2C) with average pore diameters between 135 and 540 nm (Table 4). By XRD (Figure 6) SiC particles are polycrystalline and the crystallite size (via the Scherrer equation) increases with the processing temperature from 7.1 nm in samples prepared at 1300 °C to 16.5 nm for samples processes at 1600 °C. (It is noted though that those crystallite sizes should be considered as lower limits because the (111), (220), and (311) reflections of β-SiC coincide with the (102), (110), and (116) reflections of α-SiC, causing additional broadening. Of course, the upper limit for the crystallite size would be double those values.) BET surface areas are relatively low (in the 13−22 $m^2\ g^{-1}$ range), reflecting the macroporosity and suggesting that the crystallites within the larger particles observed by SEM (80−150 nm in diameter) are closely packed with no gaps or crevices.

Although F-20-45 samples processed just at 1200 °C under Ar do not look very different than the others (Figure 9), upon oxidative removal of the residual carbon, they do have a completely different microstructure from samples processed at higher temperatures (Figure 8): they are mesoporous (average pore diameter ~20 nm), have large surface areas (~380 $m^2\ g^{-1}$), and consist of smaller particles (~5 nm in diameter). They are also amorphous by XRD. Yet, by considering their skeletal density (~2.92 $g\ cm^{-3}$) they would consist of 75% mol/mol SiC and 25% mol/mol SiO_2. Also, as shown in Figure 9, reintroducing those samples into the tube furnace and heating further at 1600 °C followed by oxidative cleaning generates the same structures observed by direct heating at 1600/600 °C (compare Figures 8 and 9). Therefore, although processing at 1200 °C is sufficient to produce SiC, it seems that grain growth occurs between 1300 and 1600 °C.

4. Discussion

All SiC samples of the F-20-30 and F-30-45 formulations shrink to about 60% of the size of the original molds, but they remain crack-free and monolithic (Figure 10).

Microscopically, after the unreacted carbon is cleaned off, samples pyrolyzed above 1300 °C look similar to one another and distinctly different from those pyrolyzed at 1200 °C. Any possible model that could be used to explain those experimental observations should address the invariance of the SiC nanomorphology above 1300 °C and rely on the current mechanistic understanding and the topology of the carbothermal process. The carbothermal reduction of eq 1 should start either as a solid−solid or even perhaps as a liquid−solid reaction between SiO_2 and C.[5a] (It is noted that although quartz melts at about 1650 °C, nanoparticulate silica in base-catalyzed silica aerogels sinters completely at 1050 °C,[29,30] implying surface melting at much lower temperatures.) Hence, the reaction between SiO_2 and C, at least initially, depends critically on the contact area between the two reactants; from that perspective, the starting material of this study has been designed specifically to turn the entire mesoporous surface of silica into a contact area with C. There, the initial elementary process between SiO_2 and C should follow eq 6

$$SiO_2(s) + C(s) \rightarrow SiO(g) + CO(g) \quad (6)$$

Once SiO(g) is formed, synthesis of SiC could follow via a gas−solid reaction with carbon:[9]

$$SiO(g) + 2C(s) \rightarrow SiC(s) + CO(g) \quad (7)$$

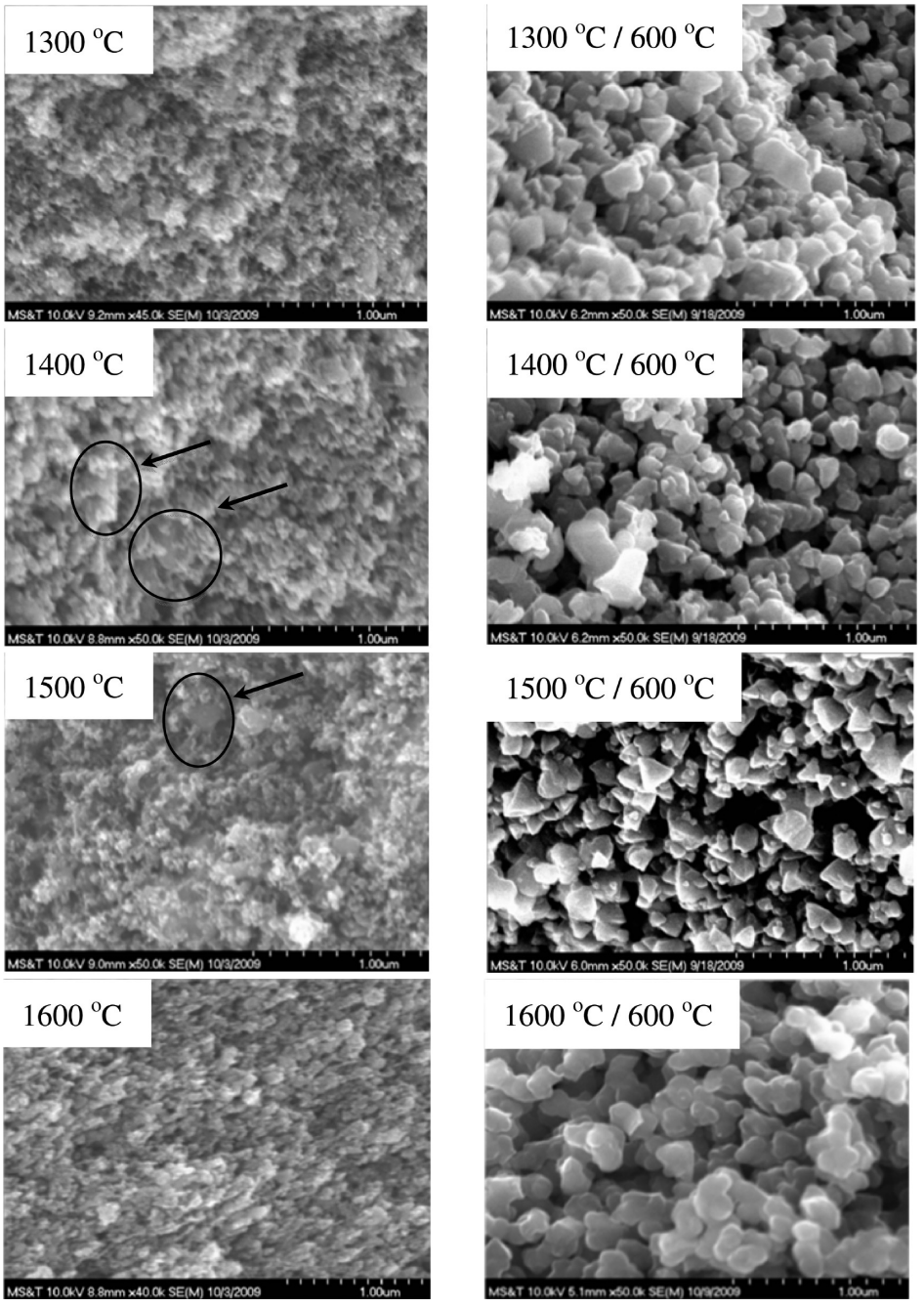

Figure 8. SEM of F-20-45 samples treated carbothermally for 72 h at the temperatures shown. Left column: samples before oxidative cleaning at 600 °C in air. SiC particles (pointed at by arrows and circles) are discernible under the "debris" on top. Right column: after removal of unreacted carbon, confirming that the debris on top was unreacted carbon (All full-scale bars at 1 μm).

CO(g) from reactions 6 and 7 reacts with silica via eq 8, producing more SiO(g)

$$SiO_2(s) + CO(g) \rightarrow SiO(g) + CO_2(g) \qquad (8)$$

whereasCO_2 comproportionates with C according to the Boudouard reaction[31−33]

$$CO_2(g) + C(s) \rightarrow 2CO(g) \qquad (9)$$

Overall, there is no sign of SiO and CO reacting in the pores via eq 2 to yield whiskers. Scheme 2 summarizes topologically the sequence of the reactions above leading to SiC. According to that model, half of the CO should escape unreacted through the carbon coating. Therefore, because subsequent gasification of SiO_2 into SiO involves reaction with CO (eq 8), for complete reaction of SiO_2, the C:SiO_2 ratio should be double of what is required stoichiometrically via eq 1, i.e., at least 6. On the basis of the ρ_s values (Table 4), the SiC content in the F-20-30 samples (C:SiO_2 = 4.4) reacted for 72 h at 1200−1600 °C is 76−93 mol percent, which is of course higher than what is expected from the model (75%), but lower than the SiC content in F-20-45

(31) Weimer, A. W.; Nilsen, K. J.; Cochran, G. A.; Roach, R. P. *AIChE J.* **1993**, *39*, 493–503.
(32) Wei, G. C.; Kennedy, C. R.; Harris, L. A. *J. Am. Ceram. Soc. Bull.* **1984**, *63*, 1054–1061.
(33) Miller, P. D.; Lee, J. G.; Cutler, I. B. *J. Am. Ceram. Soc.* **1979**, *62*, 147–149.

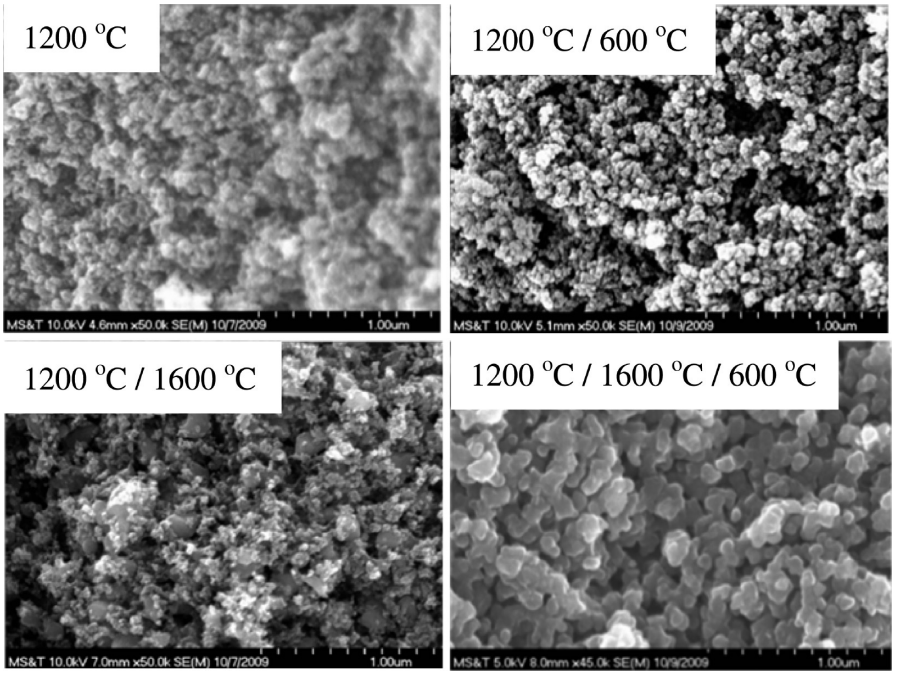

Figure 9. SEM of F-20-45 samples treated carbothermally at 1200 °C and at 1200 °C and subsequently at 1600 °C. Left column: samples before oxidative cleaning of unreacted carbon at 600 °C in air. Right column: after removal of unreacted carbon. Considering the data together with Figure 8, macroporosity and large particles are created by processes taking place between 1200 and 1300 °C (all full-scale bars at 1 μm).

Figure 10. Photographs of a F-20-45 PAN-cross-linked silica aerogel monolith (left) and the resulting SiC aerogel monolith (right) after all processing steps (i.e., aromatization at 225 °C in air, carbothermal reduction at 1400 °C under flowing Ar, and oxidative removal of unreacted carbon at 600 °C in air).

samples ($C:SiO_2 = 7.1$), where it reaches 100%. Thus, diffusion of CO through the C layer should be restricted but not completely prevented. Accordingly, a $C:SiO_2$ ratio higher than the stoichiometric ratio of 3 (refer to eq 1) is required for complete conversion of SiO_2 to SiC.

Upon closer examination, because reaction 6, which sets off the entire process, takes place at the points of contact between SiO_2 and C, once those points have been consumed, reaction 6 and all subsequent processes should stop.[31] However, as data from the F-20-45 samples show, formation of SiC can continue until complete conversion SiO_2 to SiC. Continuation of the carbothermal process

Scheme 2. Carbothermal Processes at the Interface of Silica and Carbon

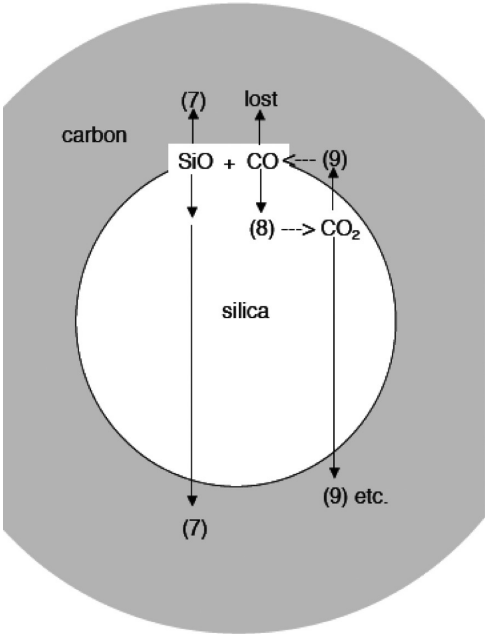

could be attributed to the solid−solid reaction of eq 10 at the points of contact of SiC with SiO_2[17,34−36]

$$SiC(s) + 2SiO_2(s) \rightarrow 3SiO(g) + CO(g) \qquad (10)$$

Equation 10 regenerates SiO(g) and it is known that it causes loss of SiC during prolonged contact with SiO_2 at high

(34) Paccaud, O.; Derré, A. *Chem. Vap. Deposition* **2000**, *6*, 33–40.
(35) Rocabois, P.; Chatillon, C.; Bernard, C. *Surf. Coat. Technol.* **1993**, *61*, 86–92.
(36) Jacobson, N. S.; Lee, K. N.; Fox, D. S. *J. Am. Ceram. Soc.* **1992**, *75*, 1603–1611.

Table 6. Characterization of SiC Aerogels Processed from PAN-Cross-Linked Aerogels without SCF CO_2 Drying[a]

sample (°C) [h]	diameter (cm)	shrinkage (%)[b]	bulk density, ρ_b (g cm^{-3})	skeletal density, ρ_s (g cm^{-3})	porosity, Π (% void space)	BET surface area, σ (m^2 g^{-1})	average pore diameter (nm)[c]	particle radius,[d] r (nm)	crystallite size[e] (nm)
				F-20-45 (C:SiO_2 = 7.08 mol:mol)					
1500 [72]	0.550	42	0.587	$3.17_8 \pm 0.01_8$	82	18	19.7 [308]	52.4	14.8 ± 1.2

[a] Data for a sample processed carbothermally at the temperature and time-period indicated, followed by oxidative removal of unreacted carbon at 600 °C in air for 5 h. [b] Shrinkage relative to the diameter of the PAN-cross-linked aerogels. [c] By the $4V_{total}/\sigma$ method. For the first number, V_{total} was calculated by the single-point adsorption method; for the number in brackets, V_{total} was calculated via $V_{total} = (1/\rho_b) - (1/\rho_s)$. [d] Calculated via $r = 3/\rho_s\sigma$. [e] By XRD using the Scherrer equation; averages from the values obtained from the (111), (220), and (311) reflections.

Scheme 3. Processes at the Interface of Silica and Newly Formed Silicon Carbide

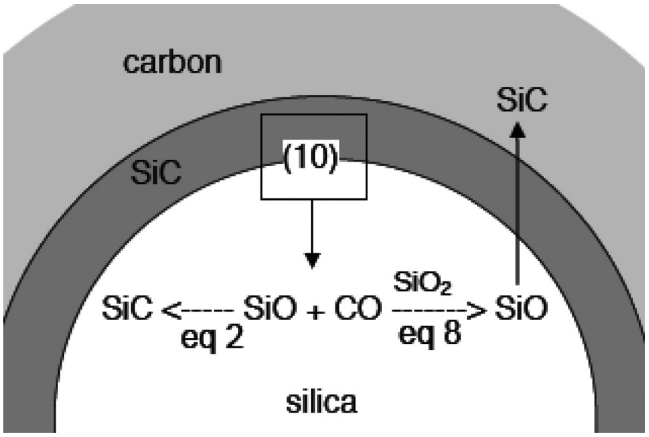

temperatures.[17] Equation 10 injects 3 mols of SiO and 1 mol of CO in the yet-unreached SiO_2 layer (Scheme 3). One mol of SiO may react with 3 mols of CO (eq 2) yielding SiC nanocrystals, whereas the remaining SiO has no other option but to diffuse through SiC and react with C as it emerges into the outer C layer, yielding SiC according to eq 7. Alternatively, CO injected into the SiO_2 layer may react with SiO_2 according to eq 8, producing more SiO. Diffusion of SiO through SiC should be slow, explaining the long reaction times. Overall, the initial SiC layer is consumed internally and grows externally in a process somewhat reminiscent of the inside out growth mechanism of certain inorganic fullerenelike layered structures.[37] The larger crystallites at higher temperatures are attributed to faster kinetics for eq 2.[28] The rather uniform SiC particle size between 1300 and 1600 °C can be explained if the silica nanoparticles melt between 1200 and 1300 °C so that new SiC crystallites get dispersed in the molten silica nanopockets wherein they are recycled through eq 10, and eventually coalesce as SiO_2 is consumed with no gaps or crevices between them. This model is not unreasonable considering together that: (a) nanoparticulate matter melts at much lower temperatures than the bulk form;[38] (b) silica aerogels undergo sintering (and therefore surface melting) at ~1050 °C; and, (c) the reaction between silica and carbon necessarily takes place at the interface of the two materials. By the same line of reasoning, SiO_2 remains solid in samples processed at 1200 °C. Consequently, amorphous SiC particles are not in full contact with SiO_2 or one another, and the SiC/SiO_2 mixtures are mesoporous with relatively high surface areas. According to this model, further heating of such samples above 1300 °C causes melting of SiO_2 and the terminal samples resume the appearance of samples processed at those temperatures from the beginning (Figure 9).

The one-step synthesis of the PAN-cross-linked silica framework is certainly a major advancement over previous work on polymer cross-linked aerogels, in which cross-linking agents had to be introduced post-gelation by time-consuming solvent exchanges.[22] However, the overall process as described above is not designed for efficiency; our focus so far has been on effecting the processes within the conformally coated silica framework. From that perspective, loose polymer in the mesopores is undesirable, and therefore the method still involves post-cross-linking washes. Now, having established that all processes happen within the conformally coated skeletal framework, we attempted to circumvent postcross-linking removal of loose PAN, reasoning that any carbon formed in the mesopores would be just a spectator removable at the final oxidation step. Furthermore, since mechanically strong polymer cross-linked aerogels can be made through ambient pressure drying,[39] we also attempted to eliminate SCF CO_2 drying at the same time. Table 6 summarizes the properties of an F-20-45 sample processed directly through aromatization, carbonization, carbothermal reduction, and oxidative cleaning of unreacted carbon without prior removal of loose PAN or SCF CO_2 drying. A comparison of the data in Table 6 with the corresponding data in Table 4 shows that the materials properties of both kinds of porous SiC are, within error, the same. Clearly, the economic advantage of this approach provides significant leverage from an applications perspective.

5. Conclusion

A polymer cross-linked aerogel has been used for the first time as the starting material in the synthesis of another porous material. Recently, polymer cross-linked interpenetrating resorcinol-formaldehyde (RF)/iron oxide

(37) See for example: (a) Chen, J.; Li, S.-L.; Gao, F.; Tao, Z.-L. *Chem. Mater*. **2003**, *15*, 1012–1019. (b) Zak, A.; Feldman, Y.; Alperovich, V.; Rosentsveig, R.; Tenne, R. *J. Am. Chem. Soc*. **2000**, *112*, 11108–11116. (c) Tenne, R.; Homyonfer, M.; Feldman, Y. *Chem. Mater*. **1998**, *10*, 3225–3238.

(38) Cao, B.; Starace, A. K.; Judd, O. H.; Jarrold, M. F. *J. Am. Chem. Soc*. **2009**, *131*, 2446–2447.

(39) Leventis, N.; Palczer, A.; McCorkle, L.; Zhang, G.; Sotiriou-Leventis, C. *J. Sol−Gel Sci. Technol*. **2005**, *35*, 99–105.

nannoparticles have been used for the pyrolytic synthesis of iron aerogels.[40] In those materials, carbothermal reduction took place between RF and iron oxide; the role of the cross-linking polymer (polyurea) was to bring the RF and iron oxide nanoparticles in better contact by melting, rendering their reaction more efficient (the onset of the reduction was decreased by 400 °C relative to the noncross-linked samples). Here, the cross-linking polymer (PAN) is the reagent, it does not melt and the 3D core−shell structure is retained through aromatization, carbonization and carbothermal reduction. To the best of our knowledge, the method described herewith is one of the most efficient in the synthesis of highly porous (70%) monolithic SiC. Si-AIBN has been used for proof-of-concept purposes only and its involvement should not be considered as deterrent. Conformal PAN coatings would be obtained with other surface-confined initiators, including monodentate ones.[41] Alternatively, such coatings could be also obtained by engaging surface-confined acrylates via homogeneous thermal or photopolymerization of AN in the mesopores.[42−44] Variants of this method are currently being explored for the synthesis of other carbides.

Acknowledgment. We thank the National Science Foundation for financial support (CHE-0809562 and CMMI-0653919). We also acknowledge the Materials Research Center of Missouri S&T for support in sample characterization (SEM and XRD). Solids NMR work was conducted at the University of Missouri Columbia by Dr. Wei Wycoff on a 300 MHz NMR instrument purchased with NSF CHE-95-31247 and NIH 1S10RR11962-01.

Supporting Information Available: Suggested definition of an aerogel (PDF). This material is available free of charge via the Internet at http://pubs.acs.org.

(40) Leventis, N.; Chandrasekaran, N.; Sotiriou-Leventis, C.; Mumtaz, A. *J. Mater. Chem.* **2009**, *19*, 63–65.
(41) See for example: Prucker, O.; Ruhe, J. *Macromolecules* **1998**, *31*, 592–601.
(42) Ilhan, U. F.; Fabrizio, E. F.; McCorkle, L.; Scheiman, D.; Dass, A.; Palczer, A.; Meador, M. A. B.; Leventis, N. *J. Mater. Chem.* **2006**, *16*, 3046–3054.
(43) Nguyen, B. N.; Meador, M. A. B.; Tousley, M. E.; Brian, S.; McCorkle, L.; Scheiman, D. A.; Palczer, A. *ACS Appl. Mater. Interfaces* **2009**, *1*, 621–630.
(44) Wingfield, C.; Baski, A.; Betrino, M. F.; Leventis, N.; Mohite, D. P.; Lu, H. *Chem. Mater.* **2009**, *21*, 2108–2114.